Glycerol Esterification for Triacetin Production using $Fe_3O_4@SiO_2@PO_4^{3-}$ as Heterogeneous Magnetic Catalyst

Amjad Ali (amjadali@thapar.edu)
Thapar Institute of Engineering and Technology https://orcid.org/0000-0002-3578-578X
Km Abida
Thapar Institute of Engineering and Technology
Ritika Jindal
Thapar University: Thapar Institute of Engineering and Technology

Research Article

Keywords: acetic acid, glycerol, phosphate, HPLC, magnetic catalyst, and triacetin

Posted Date: October 19th, 2021

DOI: https://doi.org/10.21203/rs.3.rs-879616/v1

Abstract

To facilitate the magnetic separation, phosphate group is embedded onto silica-coated Fe_3O_4 magnetic nanoparticles to prepare $Fe_3O_4@SiO_2@PO_4^{3-}$ solid catalyst for the glycerol esterification with acetic acid. The catalyst was characterized by powder X-ray diffraction (XRD), transmission electron microscopy (TEM), vibrating magnetic spectroscopy (VSM) and Fourier Transform Infrared (FTIR) spectroscopy. The $Fe_3O_4@SiO_2@PO_4^{3-}$ magnetic catalyst during the glycerol esterification with acetic acid was found to demonstrate excellent glycerol conversion levels (97 %) while retaining 92 % triacetin selectivity. The plausible mechanism of glycerol esterification suggests the initiation of the reaction by the protonation of the acetic acid. The catalyst was recovered from the reaction mixture under the influence of external magnetic field and reused during 4 consecutive reaction cycles.

1. Introduction

At the beginning of the twentieth century, biodiesel (BD) has emerged as an alternative fuel to combat the issues related to climate change, air pollution, energy demand and energy security. Ever increasing BD production also lead to generate enormous amount of crude glycerol (CGL) which would be approximately one tenth of BD produced. Disposal and purification of this excess CGL may pose serious threat to the environment and may cause water as well as soil pollution (Mufrodi et al 2020; Testa et al. 2013). Therefore, for the past few years, researchers are exploring various methods for efficient utilization of CGL (Okoye et al. 2017). The CGL possesses a meagre economic value because of the impurities present (methanol, catalyst, BD, trig-, di-, and mono-glycerides). Moreover, purification of CGL is quite expensive and may generate huge amount effluents, which is challenging to dispose of and may cause the environmental pollution (Chozhavendhan et al. 2020). One of the most suitable application of this CGL could be as precursor for the synthesis of fine chemicals for nonedible application. Glycerol (GL) esterification with acetic acid in presence of acidic acid leads to the formation of acetins viz., monoacetin (MA), diacetin (DA), and triacetin (TA) (Nda-Umar et al. 2020) as shown in scheme 1. TA has a variety of industrial application in pharmaceuticals, cosmetics, polymers, cryogenics, and fuels as an anti-knock additive for gasoline, and cold flow and viscosity improver additive for BD (Testa et al. 2019).

For TA synthesis most popular approach is homogeneous Brønsted acid (H_2SO_4, H_3PO_4, $HClO_4$ etc.) catalysed GL esterification, with acetic acid (AcA), which is a low cost eco-friendly and non-hazardous chemical in comparison to acetic anhydride (AcAn) (Nda-Umar et al. 2020). Homogeneous Acid catalysts demonstrate better reactivity and product selectivity, however, they are highly corrosive, needed neutralization and removal from the reaction mixture, and are non-reusable. Thus, effluents generated during the product washing, to remove the catalyst, need to be disposed of safely to avoid any kind of environmental pollution. To simplify the issues associated with homogeneous catalysts, many researchers, in recent past, have paid additional attention in developing heterogeneous acidic catalysts. Such catalysts are easy to separate from the reaction mixture, stable and reusable (Testa et al. 2019). In case of TA synthesis, the product selectivity was found to be a function of acidic strength of the catalyst, AcA/GL molar ratio and reaction duration. The Brønsted acidic sites (e.g. PO_4^{3-}, SO_4^{2-} etc.) in reported solid catalysts have been frequently incorporated onto the silica surface (Maria et al. 2019; Kulkarni et al. 2020). To facilitate the magnetic separation of the catalysts, Fe_3O_4 magnetic nano particles (MNPs) have been embedded within the silica shell (Caon et al. 2020). Magnetic catalysts could be removed from the reaction mixture under the influence of an external magnetic field and thus overcomes the problems of frequently applied and time consuming centrifugation and filtration procedures. Additionally, due to the nano size of catalysts, large surface area facilitates the more exposure the of active sites to impart the high catalytic activity (Ajala et al. 2020). A variety of matrix (metal oxide, silica, ion exchange resins, carbon, MNPs, and zeolite) functionalized with acidic groups (PO_4^{3-} or SO_4^{2-} etc.) have been employed for TA synthesis via GL esterification and reactivity of a few of them are summarized in Table 1.

Table 1
Activity of the literatures reported heterogeneous acidic catalysts for the GL esterification with AcA.

Catalyst	wt% (w.r.t. GL)	AcA/GL (mol/mol)	Temp (°C)	Time (h)	MA %	DA %	TA %	GLC conversion %	Catalyst reusability (# of cycles)	Reference
$Zr(SO_4)_2$	5.0	3:1	105	1.0	-	-	-	40.0	NR	Maria et al. 2019
$Zr_3(PO_4)_4$	5.0	3:1	105	1.0	-	-	-	81.0	NR	Maria et al. 2019
$Zr_4(PO_4)_2(SO_4)_5$	5.0	3:1	105	1.0	15.0	48.0	39.0	100	5	Maria et al. 2019
SiO_2-H_3PO_4	5.0	9:1	100	4.0	-	-	22.84	100	NR	Manurung et al. 2020
SO_4^{2-}@SiO_2@Fe_3O_4	5	6:1	80	0.6	-	-	100	100	6	Abida et al. 2012
$Fe_4SiW_{12}O_{40}$	6.0	3:1	60	8.0	24.0	69	7	100	NR	Silva et al 2016
Fe-Sn-Ti/SO_4^{2-}	5	-	80	0.5	-	-	99	100	4	Sun et al. 2016
$PO_4^{3-}$$SiO_2$	2.0	6:1	110	5.0	20.0	50.0	30.0	100	NR	Ghoreishi et al. 2014
SO_4^{2-}-SiO_2	2.0	6:1	110	5.0	40.0	50.0	10.0	100	NR	Ghoreishi et al. 2014
MCM-41-10Ru10Cu	8.0	10:1	120	5.0	2.4	45.2	50.4	99.1	NR	Ramalingam et al.2020
Amberlyst-45	7	3:1	70	7	68.9	29.8	1.3	75.3	NR	Jiang et al. 2019
Amberlyst-36^P	-	7:1	120	-	30	50	17	100	NR	Aghbashlo et al. 2019
S-Glycerol	-	6:1	110	2	21.0	56.0	23.0	97.0	6	Malaika et al. 2021
MS-Carbon	4.5	10.4:1	126	3	4.9	27.8	66.5	97.0	5	Nda-Umar et al. 2021
ZSM-5/MCM-41	1.5	9:1	125	24	55.9	23.4	20.7	92.6	NR	Liu at al. 2019
HZSM-5	2.65	9:1	110	4.5	-	25.7	7.7	85.6	NR	Zhou et al. 2013

w.r.t. = with respect to, GL = glycerol, AcA = acetic acid, temp = reaction temperature, MA = monoacetin, DA = diacetin, TA = triacetin, GLC = glycerol conversion, h = hour, NR = not reported, MS = mesoporous silica, S = sulfur, and P = pressure

Recently, $Zr(SO_4)_2$ and $Zr_3(PO_4)_4$ catalysts have been utilized during GL esterification to obtain up to 81 % GL conversion levels on employing 3:1 AcA/GL molar ratio and 3 wt% catalyst at 105°C reaction temperature (Maria et al. 2019). The catalyst with phosphate group was found to show better activity compared to the one with sulphate group. Testa et al. anchored both sulphate and phosphate over the zirconia surface to obtain the $Zr_4(PO_4)_2(SO_4)_5$ catalyst for the GL esterification with AcA. However, TA selectivity (39 %) was not very promising while maintaining 100 % GL conversion at 105°C within 1 h of reaction duration (Maria et al. 2019). This catalyst was reused 5 times under optimized reaction conditions; however, a decline in catalyst activity and TA/DA selectivity was observed even during the 2nd cycle. In most cases, the catalyst deactivation was associated either with the active site blockage or by the leaching of active components, such as sulphate group, from the catalyst surface (Rane et al. 2016; Yang et al. 1997). Recently, our group has prepared the magnetic catalyst by attaching the sulphate group over the silica coated magnetic (SiO_2@Fe_3O_4)

nanoparticles to prepare SO_4^{2-}@SiO_2@Fe_3O_4 catalyst. The catalyst demonstrated the excellent TA selectivity (100 %) as well GL conversion (100 %) levels, isolated under the influence of external magnetic field from the reaction mixture and reused during six consecutive reaction cycles (Abida et al. 2020).

The literature review shows that most of the heterogeneous acidic catalysts, employed in GL esterification, needed a high reaction temperature (up to 120°C) and longer reaction duration (up to 24 h) to yield high GL conversion level and higher TA selectivity. In most of the cases, the low TA selectivity and poor catalyst reusability remain issues which need to be addressed. Moreover, to the best of our knowledge, phosphate based magnetic heterogeneous catalysts have not yet been explored for the GL esterification to obtain TA. Therefore, the present study aims to develop phosphate group containing magnetic catalyst for the GL esterification to produce TA.

2. Materials And Method

2.1 Materials

All the chemicals employed in present study were used as obtained without any additional purification step. Ferrous sulphate heptahydrate (99 %), Ferric chloride hexahydrate (97 %), sodium acetate (99 %), glycerol (99 %) and acetic acid (99 %) were obtained from Loba Chemie Ltd. (India), polyethylene glycol (M W ~ 10,000) was procured from HiMedia Laboratories Pvt. Ltd. (India), ethylene glycol (99 %), isopropanol (HPLC grade) and hexane (HPLC grade) were purchased from Spectrochem Pvt. Ltd. (India), ammonia solution (25 %, v/v) was procured from Merck Life Science Pvt. Ltd. (India), ethanol (95 %), tetraethyl orthosilicate (98 %), and phosphoric acid (85 %) were obtained from Sigma Aldrich (USA).

2.2 Instrumentation

Powder X-ray diffraction data of the prepared samples was collected on a PANalytical's X'Pert Pro using Cu-Kα radiation (𝜆 = 0.15406 nm) in the 2θ range of 10 to 80°. The phases present in the samples were identified by comparing the diffraction pattern with the JCPDS (Joint Committee of the Powder Diffraction Standards) database files. The Fourier transform-infrared spectra (FTIR) spectra of the samples were recorded in a KBr matrix on an Agilent Cary-660 spectrophotometer in the range of 400–4000 cm^{-1}.

To study the nature of the catalytic acidic (Brønsted or Lewis acid) sites, the samples were saturated with pyridine at room temperature and then dried at 50°C for 2 h and further heated at 300°C in a muffle furnace for 10 min. Finally, the diffuse reflectance FTIR (DRIFT) spectra of the pyridine treated catalyst samples were recorded in KBr matrix in the mid IR range (400–4000 cm^{-1}).

The surface acidity of the samples were calculated by conducting a temperature programmed desorption study of NH_3 (NH_3-TPD) using a Microtrac-BEL Corporation BELCAT II instrument which utilizes a thermo coupled detector (TCD) for detecting the evolved gases.

The specific surface area was measured by the Brunauer–Emmett–Teller (BET) method and the pore size by the BJH method using a BEL mini-II, instrument. Prior to the analysis, the samples were heated at 100°C for 3 h under vacuum to remove any adsorbed molecules from the catalyst surface.

Scanning electron microscopy coupled with energy dispersive X-ray spectrometry (SEM-EDS) was performed on a JEOL JSM 6510LV instrument and transmission electron microscopy (TEM) images were recorded on a Hitachi 7500 instrument.

The organic products have been quantified by high-performance liquid chromatography (HPLC) over an Agilent Infinity 1200 instrument. During the analysis iso-propanol (IPA)/hexane (60/40; v/v) was employed as the mobile phase with a flow rate of 0.6 mL min^{-1}, the RX-SIL column (4.6 × 250 mm, 5 µ) as the stationary phase and the peaks were identified by using a refractive index (RI) detector. All samples were analysed by maintaining a column temperature of 35°C and injecting a fixed sample volume of 20 µL.

2.3 Preparation of Fe_3O_4 MNPs

MNPs were synthesized by following the literature reported procedure with a slight modification (Kazemifard et al. 2018). In a typical preparation, as shown in Fig. 1, 0.6 g $FeSO_4.7H_2O$, 1.16 g $FeCl_3.6H_2O$, 1 g polyethylene glycol (PEG), and 2.64 g sodium acetate were added to 50 ml of ethylene glycol. The resulted colloidal solution was stirred vigorously for 30 min at room temperature. The mixture

was then sealed into 50 mL Teflon lined stainless-steel autoclave and heated at 200°C for 24 h. After the stipulated time, the autoclave was allowed to cool down to room temperature, the supernatant was decanted off, Fe_3O_4 MNPs obtained in the form of black particles were washed with ethanol multiple times, and finally dried in the oven at 60°C for 6 h.

2.4 Preparation of $Fe_3O_4@SiO_2$

The silica coated magnetic nanoparticles ($Fe_3O_4@SiO_2$) were prepared according to the literature reported method with slight modification (Wang et al. 2015), as shown in Scheme 2a. In a typical preparation, 1 g of MNPs was suspended into 300 ml isopropanol (IPA) and 50 ml ammonia solution in a 500 ml round-bottom flask. The reaction mixture was sonicated for 15 min to disperse the MNPs. To this 5 ml tetraethyl orthosilicate (TEOS) in 30 ml of IPA was added drop-wise under constant stirring for 4 h. The prepared $Fe_3O_4@SiO_2$ MNPs were collected from the reaction mixture with the help of external magnetic force, washed with ethanol multiple times, and dried at 80°C for 4 h.

2.5 Preparation of $Fe_3O_4@SiO_2@PO_4^{3-}$

To anchor the PO_4^{3-} species group over the matrix (Scheme 2b), 0.5 g of $Fe_3O_4@SiO_2$ particles were suspended in 20 ml dichloromethane, sonicated for 30 min. To this, H_3PO_4 (0.5 ml) was added drop-wise, and the resulting reaction mixture was allowed to stir for 12 h. The phosphate impregnated MNPs ($Fe_3O_4@SiO_2@PO_4^{3-}$) were isolated, washed with ethanol multiple times, dried in air for 24 h, and finally calcined at 600°C.

2.6 Esterification of glycerol

The esterification of GL with AcA was performed in a 50 ml double necked-round bottomed flask equipped with a magnetic stirrer and temperature controller. The optimum reaction conditions for the esterification of GL was established by varying the molar ratio of AcA/GL in the range of 1–9, reaction temperature (30–100°C) and catalyst amount (1–5 wt% concerning GL). The products obtained during the reaction were quantified by the HPLC technique. A typical HPLC chromatogram of the reaction products obtained under the optimized reaction condition is shown in Fig. S1, indication a maximum of 97 % GL conversion with 92 % TA selectivity.

To evaluate the catalyst reusability, it was recovered from the reaction mixture by applying external magnetic force (Fig. 2), washed with ethanol, and calcined at 600°C. The recovered catalyst was reused four times under similar regeneration and experimental conditions.

3. Results And Discussion

3.1 X-ray diffraction (XRD)

The structure of Fe_3O_4 and $Fe_3O_4@SiO_2@PO_4^{3-}$ catalyst was characterized by X-ray diffraction technique as shown in Fig. 3. For Fe_3O_4 particles, diffraction peaks at 2θ = 30.31, 35.61, 43.27, 53.97 and 62.84 ° support the cubic phase with inverse spinel structure (JCPDS card no. 01-075-0449). In reported work, the diffraction peak for Fe_3O_4 inverse spinel phase has been observed at 2θ = 35.70 ° (Naeimi et al. 2014; Elsayed et al. 2018). Upon phosphate impregnation over the $Fe_3O_4@SiO_2$ MNPs, XRD diffraction patterns show new peaks at 2θ = 25.81, 33.06, 41.30, 64.14, and 75.91 ° corresponding to hexagonal phase of iron phosphate ($FePO_4$; JCPDS card no. 00-017-0837) and an increase in the intensity of peak at 2θ = 35.61 and 53.97 ° was observed which corresponds to monoclinic silicon phosphate (SiP_2O_7; JCPDS card no. 01-070-2245). A broad hump at 20 ° is observed (Fig. 3b), to indicate the presence of amorphous silica over these particles. The FTIR study also confirmed silica coating over the MNPs, as will be discussed in the subsequent section. The average crystallite size of the $Fe_3O_4@SiO_2@PO_4^{3-}$ particles calculated from Debye–Scherrer equation was found to be 143 nm.

3.2 FTIR Analysis

The FTIR spectrum of Fe_3O_4 particles shows a typical band at 562 cm^{-1} associated to Fe—O bond as shown in Fig. 4a (Abida et al. 2020). The incorporation of silica over these particles is supported by the appearance of a new broad band at 1063 cm^{-1} due to Si—O—Si stretching vibrations, as indicated in Fig. 4b (Pourjavadi et al. 2012; Khan et al. 2017). Incorporation of phosphate group over $Fe_3O_4@SiO_2$ is supported by the presence of new bands at 3450 and 1638 cm^{-1} related to O—H deforming vibrations of P—OH

group. The band at 813 cm^{-1} can be ascribed to P = O vibrations while at 477, 600 and 636 cm^{-1} are associated with O—P—O bending vibrations (Klahn et al 2004).

3.3 Pyridine adsorption study

In the FTIR spectra of pyridine saturated Fe_3O_4 as well as $Fe_3O_4@SiO_2$ particles (Fig. 5), a peak at 1627 cm^{-1} was observed to indicate the covalent interaction between Lewis (L) acidic sites and pyridine molecule. However, the incorporation of phosphate group over the matrix leads to the formation of Brønsted (B) acidic sites. Interaction of these sites with pyridine leads to the formation of pyridinium ion which is characterized by the band at ~ 1546 cm^{-1}. The band at ~ 1490 cm^{-1} is assigned to the interaction of pyridine on B and L sites over the catalyst surface.

3.4 NH_3-TPD analysis

The strength of acidic sites over the catalyst surface and total acidity was calculated with the help of NH_3-TPD analysis. The TPD profiles of the MNPs (Fe_3O_4), and phosphated silica coated MNPs ($Fe_3O_4@SiO_2@PO_4^{3-}$) are compared in Fig. 6. Both the samples showed a broad peak at 190 ^oC owing to the desorption of physisorbed gases from the surface of these particles. However, upon phosphate group incorporation, formation of strong acidic sites over the $Fe_3O_4@SiO_2@PO_4^{3-}$catalyst are indicated by the desorption peak at 522°C, with a total acidity of 6.51 mmol g^{-1}. In case of reported sulphated silica-zirconia or sulphated zirconia catalysts the desorption peaks in the temperature range of 100–290°C and 460–600°C indicate the presence of weak acidic and strong acidic sites, respectively, over the catalyst surface (Chen et al. 2007). Deshmane and Adewuyi, in case of sulphated zirconia catalyst, also reported the desorption peaks in the temperature range of 480 to 560°C corresponding to the strong acidic sites (Deshmane et al. 2013).

3.5 BET analysis

The nitrogen adsorption-desorption isotherms of Fe_3O_4 and $Fe_3O_4@SiO_2@PO_4^{3-}$ are shown in Fig. 7, which reveal the surface porosity and pore size behaviour of these nanoparticles. Fe_3O_4 and $Fe_3O_4@SiO_2@PO_4^{3-}$ were found to show type-IV adsorption-desorption isotherms having the H1 type hysteresis loops. The Fe_3O_4 MNPs show the hysteresis loops at p/p0 = 0.3–1.0, and relatively large pore size of 9.23 nm as measured from the BJH plot. In $Fe_3O_4@SiO_2@PO_4^{3-}$ particles, the hysteresis loop shifts to relatively low pressure of p/p0 = 0.25–0.9 with a pore size of 1.21 nm, as shown in the corresponding BJH plot. The quantity of adsorbed nitrogen also decreases upon silica and phosphate impregnation over the Fe_3O_4 MNPs due to the reduction in surface area from 28.1 m^2 g^{-1} to 9.05 m^2 g^{-1}. The decrease in the surface area could also be ascribed to the partial blockage of the silica pores due to phosphate group anchoring. Ward et al. reported that the sulphate and zirconia impregnation over the silica nanoparticles were also found to reduce the pore volume and the pore diameter due to the pore blockage of the particles (Ward et al. 2011).

3.6 Magnetization efficiency of the catalyst

The magnetic property of the magnetic particles were studied with the help of vibrating sample magnetometer (VSM). Hysteresis loops (M-H) of Fe_3O_4 and $Fe_3O_4@SiO_2@PO_4^{3-}$ was measured at room temperature (Fig. 8). All magnetic particles show the ferromagnetic behaviour with the saturation magnetization (M_S) for Fe_3O_4 and $Fe_3O_4@SiO_2@PO_4^{3-}$ at 46.04 and 30.85 emu/g^{-1}, respectively. The lower M_S value for $Fe_3O_4@SiO_2@PO_4^{3-}$ is due to the effective increase in the non-magnetic mass (silica and phosphate) over the Fe_3O_4 MNPs. As shown in Fig. 8, coercivity (H_C) (from 32 to 31.17 G) and retentivety (M_R) (from 2.16 to 1.48 emu/g^{-1}) values also decrease with the phosphate and silica loading over the MNPs. Owing to the strong magnetization of $Fe_3O_4@SiO_2@PO_4^{3-}$ (30.85 emu g^{-1}) it is possible to separate it out from the reaction mixture by applying external magnetic force. These observations were quite similar to the reports by Naeimi and Nazif for the Fe_3O_4 magnetic catalyst, where M_S value decreased (from 50.86 to 15 emu/g^{-1}) after incorporating sulphonic acid over the silica coated Fe_3O_4 particles (Naeimi et al. 2013; Dong et al. 2020). Goyal et al. also reported that saturation magnetization of $CoFe_2O_4$ (19.4 emu/g^{-1}) decreases upon the non-magnetic aluminium coating over the $CoFe_2O_4$ MNPs (3.7 emu/g^{-1}) (Goyal et al 2017).

3.7 SEM and TEM analysis

The surface morphology of Fe_3O_4 and $Fe_3O_4@SiO_2@PO_4^{3-}$ was compared by SEM technique, as shown in Fig. 9. The SEM images of the Fe_3O_4 (Fig. 9a) show the formation of ~ 100 nm sized spherical particles which undergo the clustering to form particles of irregular geometry upon phosphate and silica incorporation over Fe_3O_4 (Fig. 9b). The TEM analysis shows that Fe_3O_4 spheres (Fig. 9c) are the clusters of ~ 147 nm sized particles. While $Fe_3O_4@SiO_2@PO_4^{3-}$ agglomerates are also made up of spherical particles (~ 156 nm) as shown in Fig. 9d. The silica coating of 10.58 nm thickness over Fe_3O_4 particles could also be observed (Fig. 9d). The crystallite size (143 nm) of $Fe_3O_4@SiO_2@PO_4^{3-}$ particles calculated from the XRD data is close to the particle size (156 nm) calculated from the TEM imaging to confirm the formation of nano sized catalyst particles.

3.8 Catalyst Screening

The catalytic activity of $Fe_3O_4@SiO_2@PO_4^{3-}$ catalyst was investigated for the GL esterification with AcA. The reaction parameters screened includes, AcA/GL molar ratio, reaction temperature, reaction duration, and catalyst amount for obtaining the best catalytic activity. In order to demonstrate the necessity of the catalyst and its various component, various blank and control experiments were performed during the GL esterification (Fig. 10). For instance, GL esterification performed either in absence of catalyst or in presence of bare MNPs/silica coated MNPs, was found to yield negligible GL conversion levels into acetins. However, GL acetylation in presence of $Fe_3O_4@SiO_2@PO_4^{3-}$ catalyst under optimized reaction conditions was found to yield almost ~ 97 % GL conversion with 92 % TA selectivity (Fig. 10). These experiments clearly underline the role of phosphate group as a catalytically active species during the GL esterification. These observations could also be correlated with the literature reports, where Ma and co-workers suggested that impregnation of Brønsted acid, sulphate group, over titanium coated MNPs was found to impart the esterification activity of the catalyst (Ma et al. 2011).

During esterification of GL with AcA, one or more -OH groups of the GL molecule can react with AcA. Therefore, up to three esters *viz.*, MA, DA and TA may be formed depending on the conditions set for the reaction. In order to optimize the reaction parameters to achieve the maximum TA selectivity, out of reagent ratio, catalyst concentration, reaction duration and reaction temperature, one variable has been changed at a time as discussed below. The catalyst performance was evaluated on the basis of percentage GL conversion (= moles of all the products/moles of GL taken) × 100) and percentage TA selectivity (= moles of TA/moles of all the products) × 100).

3.8.1 AcA/GL molar ratio

The influence of AcA/GL ratio on the GL esterification over the prepared catalyst was investigated by performing the reaction in the presence of 5 wt% catalyst (with respect to GL) at 80°C, for 80 min and varying the AcA/GL molar ratio 1:1 to 9:1 (Fig. 11a). It can be observed that at 3:1 AcA/GL molar ratio, MA was found to be the main product, which gradually decreases while the TA selectivity increases as the reactant ratio was increased from 3:1 to 6:1. At reactant ratio of 6:1, the observed GL conversion was as high as 97 % and selectivity towards TA was found to be ~ 92 %. A further rise in the AcA/GL ratio was not found to enhance the TA selectivity or GL conversion levels. In earlier reports, the sulphate functionalized CeO_2-ZrO_2 employed for the GL esterification with AcA (Kulkarni et al. 2020). During the study, the catalyst was found to yield higher MA selectivity (52 %) but lower TA selectivity of 5 % while employing AcA/GL molar ratio of 3 at 100°C for 3 h of reaction duration. The TA selectivity gradually increases with increase in AcA concentration and at 10 molar ratio of AcA/GL, TA selectivity was found to be 34 % along with 99.12 % GL conversion.

3.8.2 Catalyst amount

Figure 11b shows the influence of catalyst amount over GL conversion and selectivity towards MA, DA and TA when the reaction was performed for 80 min, at AcA/GL molar ratio of 6:1, at reaction temperature 80°C and varying the catalyst amount from 1 to 7 wt% (concerning GL). From the result, it was observed that GL conversion increased sharply along with catalyst amount, from 0 to 5 wt%, and then remained constant from 5 wt% to 7 wt%. At 1 wt%, MA was the main product which decreases gradually on increasing the catalyst amount. Thus, the TA selectivity was found to be maximum, 92 %, at 5 wt% catalyst amount in the reaction mixture. In case of AcA/GL (10:1 molar ratio) esterification in the presence of SO_4^{2-}/CeO_2-ZrO_2 catalyst, the TA selectivity was found to increase gradually from 7.32 to 21.26 % with the increase in catalyst amount (from 1 to 5 wt%, concerning GL) (Kulkarni et al. 2020). Thus extent of GL esterification as well TA selectivity was found to be a function of active (acidic) sites, which would be more at higher catalyst concentration in the reaction mixture.

3.8.3 Reaction temperature

The GL esterification was found to be endothermic in nature and hence, a higher reaction temperature favours the esterification to obtain TA (Li et al.2020). The effect of reaction temperature over acetin selectivity and GL conversion was studied by performing the reaction in presence of 5 wt% catalyst (concerning GL), AcA/GL molar ratio 6:1, at 80 min and varying the reaction temperature from 35 to 100°C as shown in Fig. 11c. At room temperature (35°C), the major product formed was MA which decreases with increasing temperature. As the temperature is increased to 80°C, the TA selectivity touches the highest value of 92 % and remains the same even at an elevated temperature of 100°C. Dizoglu and Sert also reports the same observation, while studying the activated carbon/UiO-66 as catalyst for GL esterification with AcA employing 6 wt% of catalyst amount, 6:1 of AcA/GL molar ratio, while the optimum temperature was being 90°C to obtain the TA selectivity of 17.9 % (Dizoglu and Sert 2020). In the literature, very few reports claim ≥ 90 % TA selectivity (Abida et al. 2020; Sun et al. 2016). At a high reaction temperature (110°C) the formation of the acylium ion from AcA was found to be facilitated which ultimately acts as the source of acetylating agent for the acetin formation from GL (Malaika et al. 2021; Nda-Umar et al. 2020).

3.8.4 Reaction duration

An increase in reaction time also found to influence the acetin selectivity when the reaction was performed in the presence of 5 wt% catalyst (concerning GL) at 80°C, employing AcA/GL molar ratio of 6:1 and varying the reaction time from 20 to 80 min as shown in Fig. 11d. As expected, the conversion of GL into acetins gradually increases with the reaction duration. On increasing the reaction time from 0 to 60 min, the selectivity of MA and DA increases gradually while the TA concentration almost remains constant. After 80 min, the TA selectivity reaches the maximum value of 92 % at the expense of MA and DA. A further increase in reaction duration, upto 100 min, was not found to increase the TA selectivity. The observation is indicating the stepwise GL esterification involving the formation of MA initially followed by DA and TA. Magar et al. studied the extent of GL esterification at various time intervals employing modified heteropoly acid as a catalyst at 110 ^{o}C utilizing 20:1 AcA/GL molar ratio. They observed 30 %, 42 % and 23 % selectivity of MA, DA, and TA, respectively, in 2 h of reaction duration (Magar et al. 2020). However, the DA and TA selectivity was found to increase to 54 % and 34 %, respectively, while the MA selectivity reduced to 12 % after 6 h of reaction duration. Thus our study as well as literature report supported the stepwise GL esterification and increase in DA and TA yield on increasing the reaction duration. Thus, the study supports that three –OH groups of GL are esterified in a stepwise fashion.

3.9 Reusability study

The ease of catalyst separation and reusability are the main advantages of heterogeneous catalysts over homogeneous one. The magnetic catalyst was employed for the GL esterification under the optimized reaction conditions and after the completion of the reaction; it was removed from the reaction mixture under the influence of an external magnetic field as shown in Fig. 1. The recovered catalyst was washed with ethanol, dried, and calcined at 600°C for 3 h. The regenerated catalyst was further reused during four cycles under similar regeneration and experimental conditions. During the reusability experiments, the TA selectivity was found to decline up to 42 % in the second cycle and then remain 20 % during the next two consecutive cycles (Fig. 12). The reason for the decline in catalyst activity may be the leaching of the active sites from the catalyst surface.

The XRD spectra (Fig. 13) of fresh and reused catalysts revealed that the PO_4^{3-} moiety has partially detached from the catalyst surface. A comparison of EDX data of fresh and reused catalyst (Fig. S2) also supports the decrease in phosphorous contents (from 10.7 % to 1.6 %) in the used catalyst, to indicate the loss of phosphate group from the catalyst upon its successive reuse. Thus, catalyst decomposition was found to be the primary reason behind the loss in its activity.

3.10 Proposed mechanism for the GL esterification with AcA

GL esterification in absence of catalyst resulted in partial conversion levels into acetins even after a prolonged reaction duration of 4.5 h. However, in the presence of the magnetic $Fe_3O_4@SiO_2@PO_4^{3-}$ catalyst, reaction duration of 80 min is required to achieve 97 % GL esterification. This observation indicates that phosphate group is the catalytically active species in the GL esterification with AcA. Homogeneous phosphoric or sulfuric acid catalyzed esterification of mono- as well tri-alcohol (GL) has been reported to follow the first-order kinetic model (Beula et al. 2013). In such reactions, the rate of the reaction was found to be a function of AcA concentration. During the present study when the AcA concentration was varied, TA selectivity was also found to fluctuate. However, the same was not found to be effected when the GL concentration was varied. The effect of time on the course of reaction indicates the stepwise esterification of –OH groups of GL.

On the basis above mentioned experimental study as well literature reports, the plausible mechanism should involve the protonation of the AcA, to form a carbocation (II), in the first step (Kong et al. 2016) where the proton is furnished by the magnetic heterogeneous acidic catalyst as shown in Scheme 3. Now, carbocation (II), reacts with one alcoholic –O–H group of GL to form intermediate (III). A water molecule has been given away by intermediate (III) to generate a new carbocation (IV) which ultimately disintegrate into catalyst and MA (V). The remaining two alcoholic groups of the MA would react with AcA, following a similar mechanism as described above, to form a TA molecule.

4. Conclusions

A Brønsted acid based heterogeneous acidic magnetic catalyst (Fe_3O_4@SiO_2-PO_4^{3-}) was prepared for the glycerol esterification with acetic acid. The glycerol esterification was performed over various concentrations of acetic acid/glycerol (1–9) and various temperatures (35–100°C). The results showed that it is essential to use excess amount of acetic acid to attain the highest glycerol conversion as well as TA selectivity. A 97 % GL conversion with 92 % TA selectivity was obtained using the Fe_3O_4@SiO_2-PO_4^{3-} catalyst at 80°C for 80 min while employing 5 wt% of catalyst amount. The catalyst was separated from the reaction mixture under the influence of a magnetic field and reused during the four reaction cycles. Efforts are in progress to further improve the catalyst stability and reusability.

Declarations

Acknowledgements: We acknowledge CSIR for the financial support (Ref No.: 01(2964)/18/EMR-II), DST-FIST (Ref. No. SR/FST/CSI-217/2010) for funding instrumentation facility in the School of Chemistry and Biochemistry. We are also thankful to SAI Lab for SEM-EDX and XRD analysis and Prof. B. N. Chudasma for VSM analysis.

Data availability: The datasets used and/or analyzed during the current study are available from the corresponding author on reasonable request.

Ethics approval and consent to participate: Not applicable

Consent for publication: Not applicable

Competing interests: The authors declare no competing interests.

Authors' contributions: RJ performed the experimental work and analysed the data. KA performed the reusability study, data analysis and preparedfirst draft of the manuscript. AA conceptualized the scheme, guided the students and corrected the manuscript draft. All authors read and approved the final manuscript.

References

1. Ajala EO, Ajala MA, Ayinla IK, Sonusi AD, Fanodun SE (2020) Nano-synthesis of solid acid catalysts from waste-iron-flling for biodiesel production using high free fatty acid waste cooking oil. Sci Rep 10:13256. https://doi.org/10.1038/s41598-020-70025-x
2. Abida K, Ali A (2020) Sulphuric acid-functionalized siliceous zirconia as an efficient and reusable catalyst for the synthesis of glycerol triacetate. Chem Papers 74:3627–3639. https://doi.org/10.1007/s11696-020-01189-z
3. Abida A, Chudasama B, Ali A (2020) Development and Functionalization of Magnetic Nanoparticles as Stable and Reusable Catalyst for Triacetin Synthesis. New J Chem 44:9365-9376. DOI: 10.1039/d0nj00488j
4. Aghbashlo M, Tabatabaei M, Jazinid H, Ghaziaskar HS (2018) Exergoeconomic and exergoenvironmental co-optimization of continuous fuel additives (acetins) synthesis from glycerol esterification with acetic acid using Amberlyst 36 catalyst. Energy Con Manag 165:183–194. https://doi.org/10.1016/j.enconman.2018.03.054.
5. Beula C, Sai PST (2013) Kinetics of esterification of palmitic acid with ethanol-optimisation using statistical design of experiments – Int. J Chem Eng Appl 6:388-392.
6. Chozhavendhan S, Devi GK, Bharathiraja B, Kumar RP, Elavazhagan S, (2020) 9-Assessment of crude glycerol utilization for sustainable development of biorefineries, Refining Biomass Residues for Sustain Energy Bioproducts 195-212. DOI:

10.1016/B978-0-12-818996-2.00009-0

7. Caon NB, Cardoso CS, Faita FL, Vitali L, Luis Parize LS (2020) Magnetic solid-phase extraction of triclosan from water using n-octadecyl modified silica-coated magnetic nanoparticles. J Environ Chem Eng 8(4): 104003. https://doi.org/10.1016/j.jece.2020.104003
8. Cheng M, Xie W, Zong B, Sun B, Qiao M (2013) When Magnetic Catalyst Meets Magnetic Reactor: Etherification of FCC Light Gasoline as an Example. Sci Reports 9:1973. DOI: https://doi.org/10.1038/srep01973
9. Chen X, Ju Y, Mou C (2007) Direct Synthesis of Mesoporous Sulfated Silica-Zirconia Catalysts with High Catalytic Activity for Biodiesel via Esterification. J Phys Chem C 111:18731–18737. https://doi.org/10.1021/jp0749221
10. Dong Y, Han WJ, Choi HJ (2020) Additive Effect of Rod-like Magnetite/sepiolite Composite Particles on Magnetorheology. J Ind Eng Chem 93:210-215. doi:10.1016/j.jiec.2020.09.025
11. Dai Y, Wang Y, Chen C (2018) Synthesis and characterization of magnetic $LiFe_5O_8$-$LiFeO_2$ as a solid basic catalyst for biodiesel production. Catal Commun 106:20–24. https://doi.org/10.1016/j.catcom.2017.12.002
12. Deshmane VG, Adewuyi YJ (2013) Mesoporous nanocrystalline sulfated zirconia synthesis and itsapplication for FFA esterification in oils. Appl Catal A 463:196–206. http://dx.doi.org/10.1016/j.apcata.2013.05.005
13. Dizoglu G, Sert E (2020) Fuel additive synthesis by acetylation of glycerol using activated carbon/UiO-66 composite materials. Fuel 281:118584. https://doi.org/10.1016/j.fuel.2020.118584
14. Elsayed I, Mashaly M, Eltaweel F, Jackson MA, Hassan EB (2018) Dehydration of glucose to 5-hydroxymethylfurfural by a core-shell Fe_3O_4@SiO_2-SO_3H magnetic nanoparticle catalyst. Fuel 221:407–416. https://doi.org/10.1016/j.fuel.2018.02.135
15. Ghoreishi B, Asim N, Yarmo MA, Samsudin MW (2014) Mesoporous phosphated and sulphated silica as solid acid catalysts for glycerol acetylationChem Papers 68(9):1194–1204. doi: 10.2478/s11696-014-0550-x
16. Goyal A, Bansal S, Chudasama B, Tikoo KB, Kumard V, Singhal S (2017) Augmenting the catalytic performance of spinel nanoferrites ($CoFe_2O_4$ and $NiFe_2O_4$) via incorporation of Al in to the lattice. New J Chem 7(41):8320. doi: 10.1039/c7nj01486d
17. Jiang J, Li X, Zhao H, Hou Z (2019) Esterification of glycerol with acetic acid over SO3H-functionalized phenolic Resin. Fuel 255: 115842. https://doi.org/10.1016/j.fuel.2019.115842
18. Karnjanakom S, Maneechakr P, Samart C, Guan G (2018) Ultrasound-assisted acetylation of glycerol for triacetin production over green catalyst: A liquid biofuel candidate. Energy Con Manag 173:262–270. https://doi.org/10.1016/j.enconman.2018.07.086
19. Kulkarni RM, Britto PJ, Narula A, Saqline S, Anand D, Bhagyalakshmi CN, Herle R (2020) Kinetic studies on the synthesis of fuel additives from glycerol using CeO_2–ZrO_2 metal oxide catalyst. Biofuel Res J 5:1100-1108. DOI: 10.18331/BRJ2020.7.1.2
20. Kazemifard S, Nayebzadeh H (2018) Naser Saghatoleslami1 & Ebrahim Safakish, Assessment the activity of magnetic KOH/Fe_3O_4@Al_2O_3 core–shell nanocatalyst in transesterification reaction: effect of Fe/Al ratio on structural and performance. Environ Sci Pollution Res 25:32811–32821 https://doi.org/10.1007/s11356-018-3249-7
21. Khan S, Kaur G, Singh K (2017) Effect of ZrO_2 on dielectric, optical and structural properties of yttrium calcium borosilicate glasses. Ceram Int 43:722–727. https://doi.org/10.1016/j.ceramint.2016.09.219
22. Klahn M, Mathias G, Kotting C, Nonella M, Schlitter J, Gerwert KP (2004) IR Spectra of Phosphate Ions in Aqueous Solution: Predictions of a DFT/MM Approach Compared with Observations. Tavan J Phys Chem A 108(29):6186-6194. https://doi.org/10.1021/jp048617g
23. Kong PS, Aroua MK, Daud WMA, Lee HV, Cognetc P, Peres Y (2016) Catalytic Role of Solid Acid Catalysts in Glycerol Ac etylation for the Production of Bio additive: A Review RSC Adv 6:68885. https://doi.org/10.1039/C6RA10686B
24. Liu J, Wang Z, Sun Y, Jian R, Jian P, Wang D (2019) Selective synthesis of triacetin from glycerol catalyzed by HZSM-5/MCM-41 micro/mesoporous molecular sieve. Chin J Chem Eng 27:1073–1078. DOI: 10.1016/j.cjche.2018.09.013
25. Li X, Zhang J, Song Y, Ji Y, Younas M, He B (2020) Esterification of glycerol with acetic acid using a sulfonated polyphenylene sulphide non-woven fabric as a catalyst. Int J Chem React Eng 18:12. https://doi.org/10.1515/ijcre-2020-0171
26. Mufrodi Z, Astuti E, Syamsiro M, Santosa B, Sutaiman, Purwono S (2020) Triacetin Synthesis as Bio-Additive from Glycerol Using Homogeneous and Heterogeneous Catalysts. Key Eng Mater 849:90-95. doi.org/10.4028/www.scientific.net/KEM.849.90
27. Maria LT, Valeria LP, Farah M, Fatiha O, Mohamed K, Mahfoud Z, Leonarda FL (2019) Use of Zirconium Phosphate-Sulphate as Acid Catalyst for Synthesis of Glycerol-Based Fuel Additives. Catalysts 9:148. doi:10.3390/catal9020148

28. Manurung R, Anggreawan MD, Sireg AG (2020) Triacetin production using SiO_2-H_3PO_4 catalysts derived from bamboo leaf biomass waste for esterification reactions of glycerol and acetic acid. Mat Sci Eng 801:012052. doi:10.1088/1757-899X/801/1/012052
29. Malaika A, Ptaszynska K, Kozłowski M (2021) Conversion of renewable feedstock to bio-carbons dedicated for the production of green fuel additives from glycerol. Fuel 288:119609. DOI: 10.1016/j.fuel.2020.119609
30. Ma L, Li J, Ke R, Fu L 2011 Catalytic Performance, Characterization, and Mechanism Study of $Fe_2(SO_4)_3/TiO_2$ Catalyst for Selective Catalytic Reduction of NOx by Ammonia. J Phys Chem C 115:7603–7612. https://doi.org/10.1021/jp200488p
31. Magar S, Mohanraj GT, Jana SK, Rode CV (2020) Synthesis and characterization of supported heteropoly acid: Efficient solid acid catalyst for glycerol esterification to produce biofuel additives. Inorg Nano-Met Chem 50(11):1157-1165. https://doi.org/10.1080/24701556.2020.1737817
32. Nda-Umar UI, Ramli I, Muhamad EN, Azri N, Taufiq-Yap YH (2020) Optimization and Characterization of Mesoporous Sulfonated Carbon Catalyst and Its Application in Modeling and Optimization of Acetin Production. Molecules 25:5221. doi:10.3390/molecules25225221
33. Naeimi N, Mohamadabadi S (2014) Sulfonic acid-functionalized silica-coated magnetic nanoparticles as an efficient reusable catalyst for the synthesis of 1-substituted 1H-tetrazoles under solvent-free conditions†. Dalton Trans 43:12967. DOI: 10.1021/acs.jpcc.5b08743
34. Naeimi H, Nazif ZS (2013) A highly efficient nano-Fe_3O_4 encapsulated-silica particles bearing sulfonic acid groups as a solid acid catalyst for synthesis of 1,8-dioxo-octahydroxanthene derivatives. *J Nanopart Res* 15, 2026. doi: 10.1007/s11051-013-2026-2
35. Nda-Umar UI, Ramli IB, Muhamad EN, Azri N, Amadi UF, Taufiq-Yap YH (2020) Influence of Heterogeneous Catalysts and Reaction Parameters on the Acetylation of Glycerol to Acetin: A Review. Appl Sci 10:7155. doi:10.3390/app10207155
36. Okoye PU, Abdullah AZ, Hameed BH (2017) Synthesis of oxygenated fuel additives via glycerol esterification with acetic acid over bio-derived carbon catalyst. Fuel 209:538-544. http://dx.doi.org/10.1016/j.fuel.2017.08.024
37. Pourjavadi A, Hosseini SH, Doulabi M, Fakoorpoor SM, Seidi F (2012) Multi-Layer Functionalized Poly(Ionic Liquid) Coated Magnetic Nanoparticles: Highly Recoverable and Magnetically Separable Brønsted Acid Catalyst. ACS Catal 2:1259–1266. https://doi.org/10.1021/cs300140j
38. Rane SA, Pudi SM, Biswas P (2016) Esterification of Glycerol with Acetic Acid over Highly Active and Stable Alumina-based Catalysts: A Reaction Kinetics Study. Chem Biochem Eng Q 30(1):33–45. doi: 10.15255/CABEQ.2014.2093
39. Ramalingam RJ, Appaturi JN, Pulingam T, Al-Lohedan HA, Al-dhayan DM (2020) In-situ incorporation of ruthenium/copper nanoparticles in mesoporous silica derived from rice husk ash for catalytic acetylation of glycerol. Renew Energy 160:564-574. https://doi.org/10.1016/j.renene.2020.06.095
40. Silva MJD, Liberto NA, Leles LD, Pereira UA (2016) $Fe_4(SiW_{12}O_{40})$ catalyzed glycerol acetylation: Synthesis of bio additives by using highly active Lewis acid catalyst. J Mol Catal A: Chem 422:69–83. https://doi.org/10.1016/j.molcata.2016.03.003
41. Sun J, Tong X, Yu L, Wan J (2016) An efficient and sustainable production of triacetin from the acetylation of glycerol using magnetic solid acid catalysts under mild conditions. Catal Today 264:115-122. http://dx.doi.org/10.1016/j.cattod.2015.07.011
42. Testa ML, Parola VL, Liotta LF, Venezia AM (2013) Screening of different solid acid catalysts for glycerol acetylation. J Mol Catal A 367:69–76. http://dx.doi.org/10.1016/j.molcata.2012.10.027
43. Testa ML, Parola VL, Mesrar F, Ouanji F, Kacimi M, Ziyad M, Liotta LF (2019) Use of Zirconium Phosphate-Sulphate as Acid Catalyst for Synthesis of Glycerol-Based Fuel Additives. Catalysts 9(2):148. doi:10.3390/catal9020148
44. Wang J, Liang Y, Wang S, Okoye PU, Chen H, Zhou Y, Xu J, Meng Z, Wang L, Li S (2020) Using Diaper Waste to Prepare Magnetic Catalyst for the Synthesis of Glycerol Carbonate. Int J Poly Sci 4:1-9. https://doi.org/10.1155/2020/9403714
45. Wang Y, Yang X, Xu J, Wang H, Wang Z, Zhang Z, Wang S, Liang J (2019) Biodiesel production from esterification of oleic acid by a sulfonated magnetic solid acid catalyst. Renew. Energy 139, 688-695. DOI: 10.1016/j.renene.2019.02.111
46. Wang H, Covarrubias J, Prock H, Wu X, Wang D, Bossmann SH (2015) Acid-Functionalized Magnetic Nanoparticle as Heterogeneous Catalysts for Biodiesel Synthesis. J Phys Chem C 119(46):26020-26028.
47. Ward AJ, Pujari AA, Costanzo L, Masters AF, Maschmeyer T (2011) Ionic liquid-templated preparation of mesoporous silica embedded with nanocrystalline sulfated Zirconia. Nanoscale Res Lett 6:192. https://doi.org/10.1186/1556-276X-6-192

48. Yang T, Chang T, Yeh C (1997) Acidities of sulfate species formed on a superacid of sulfated Alumina. J Mol Catal A: Chem 115:339. https://doi.org/10.1016/S1381-1169(96)00283-X
49. Zhou L, Al-Zaini E, Adesina AA (2013) Catalytic characteristics and parameters optimization of the glycerol acetylation over solid acid catalysts. Fuel 103:617–625. https://doi.org/10.1016/j.fuel.2012.05.042

Figures

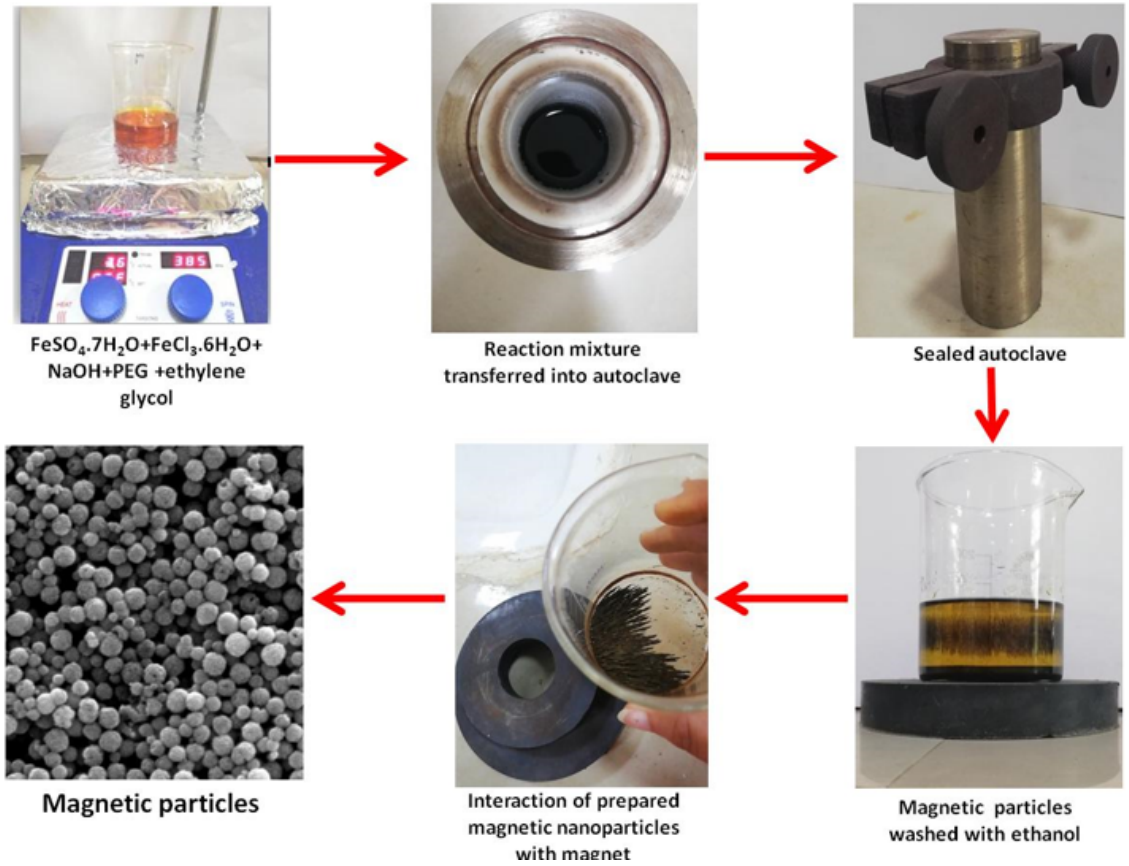

Figure 1

Preparation method of Fe3O4 magnetic nanoparticles.

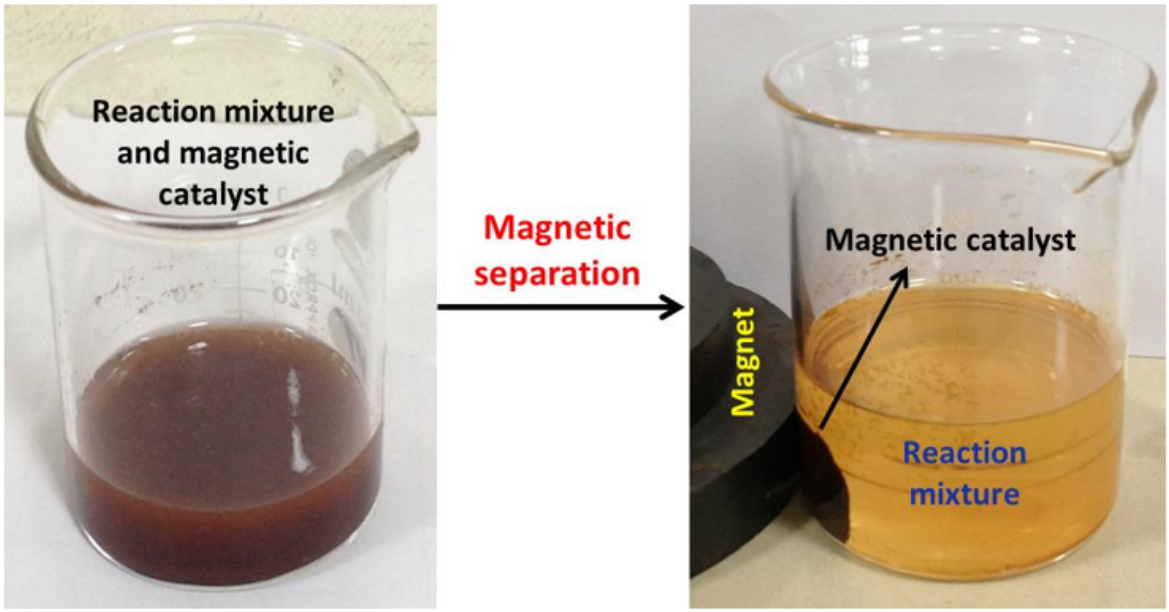

Figure 2

Separation of the magnetic catalyst with the help of external magnetic force.

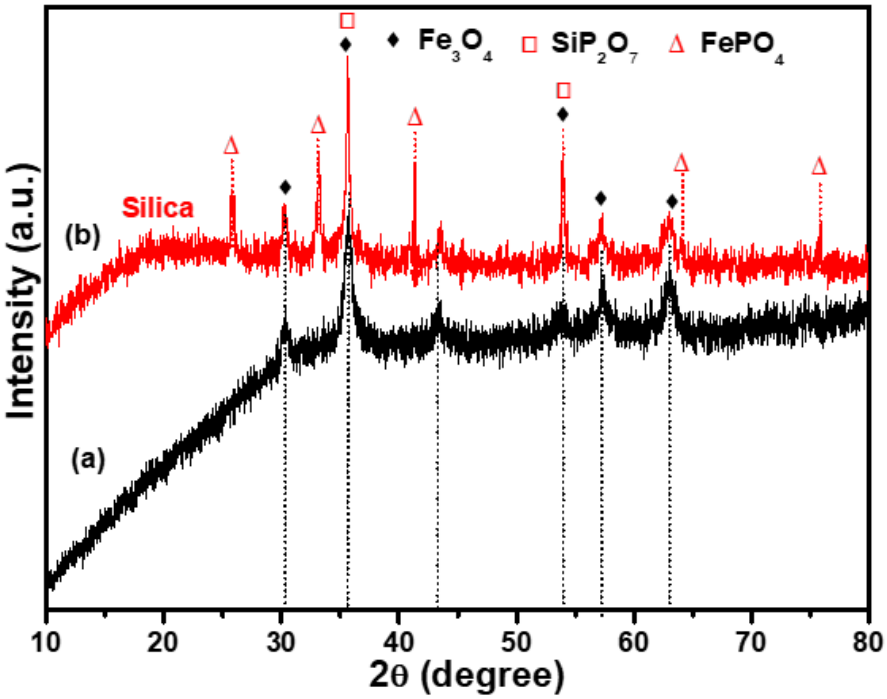

Figure 3

X-ray diffraction analysis of (a) Fe3O4, and (b) Fe3O4@SiO2@PO43-.

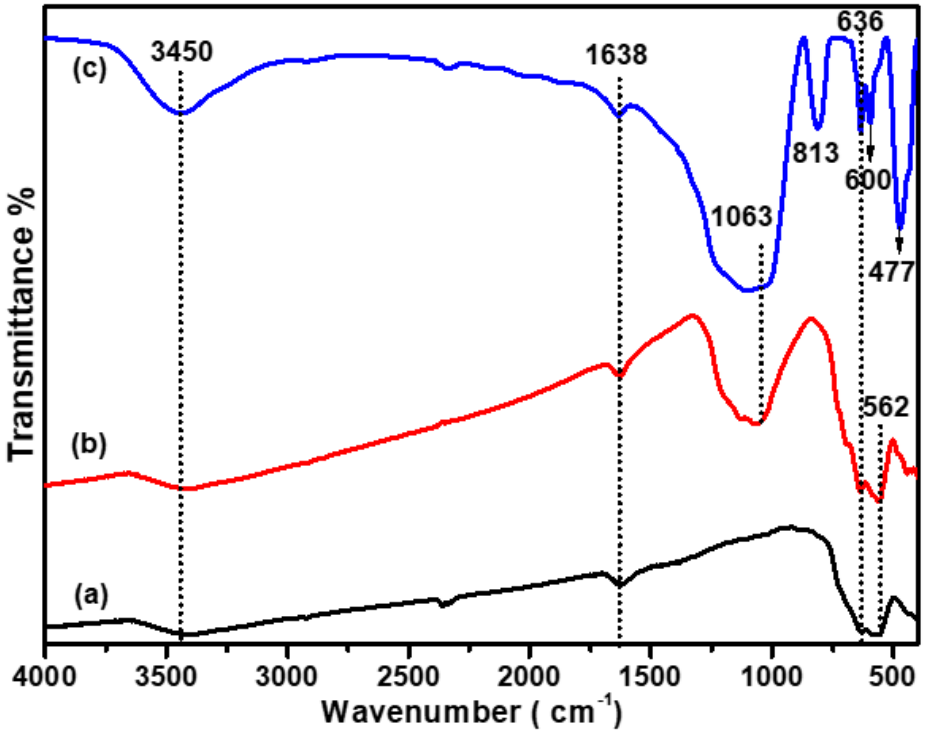

Figure 4

The FTIR spectra of the synthesized (a) Fe3O4, (b) Fe3O4@SiO2 and (c) Fe3O4@SiO2-PO43-.

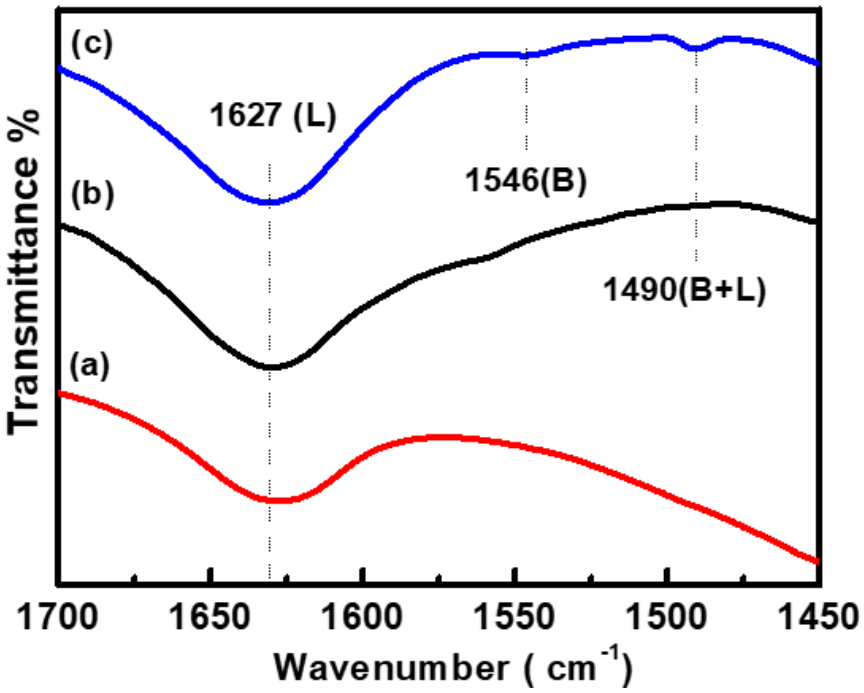

Figure 5

FTIR spectra of pyridine adsorbed on (a) Fe3O4, (b) Fe3O4@SiO2 and (c) Fe3O4@SiO2@PO43-.

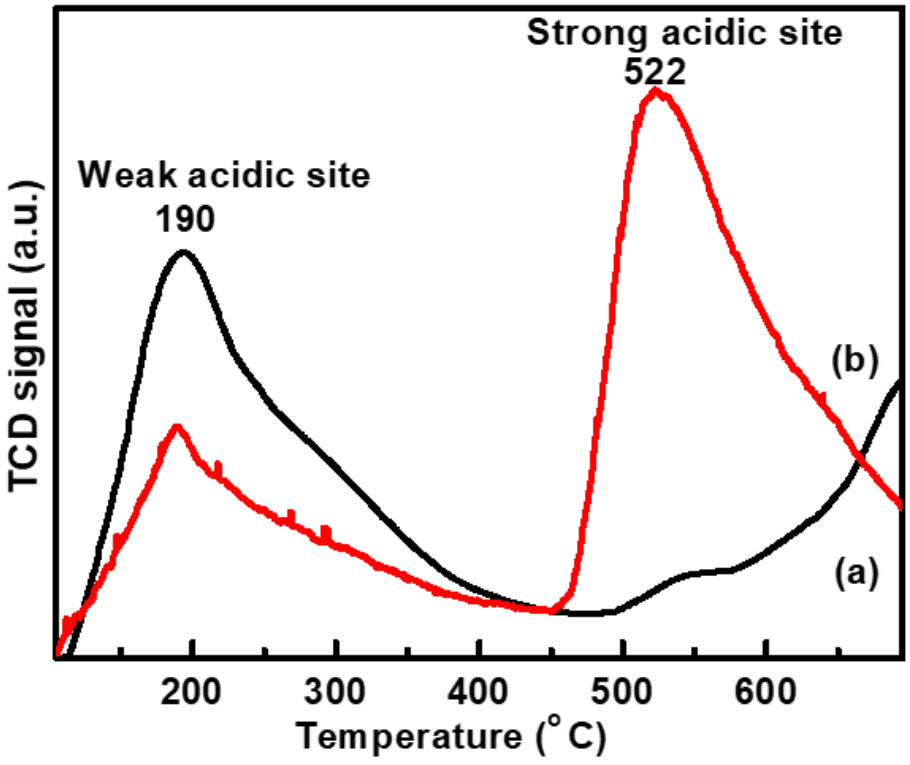

Figure 6

NH3-TPD profiles for (a) Fe3O4, and (b) Fe3O4@SiO2@PO43-.

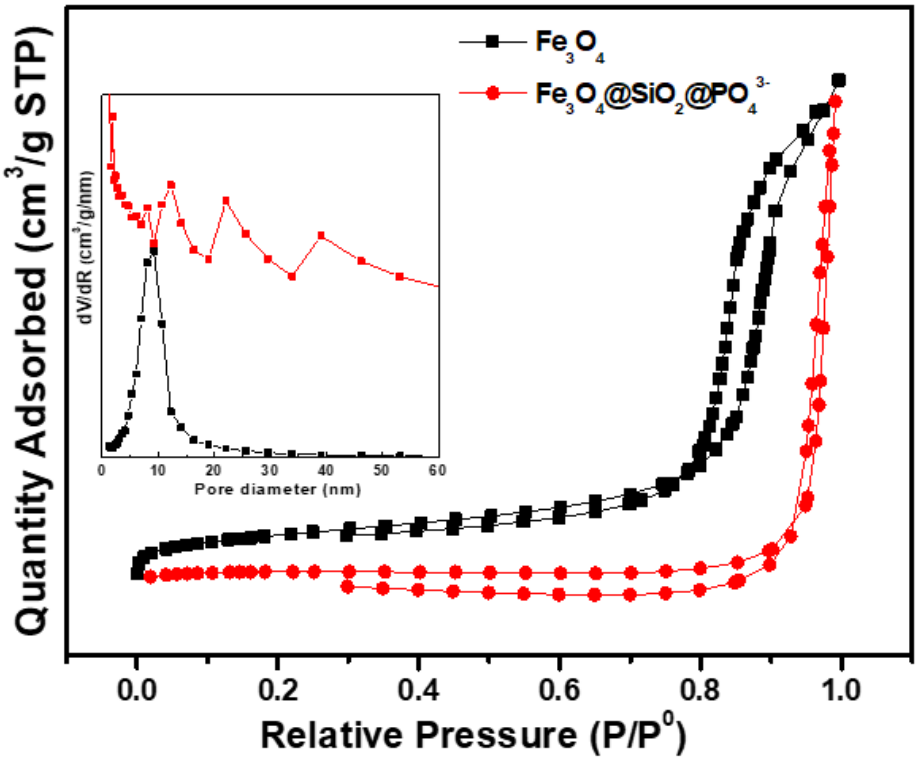

Figure 7

N2 adsorption-desorption isotherms and Pore distribution branch of the nitrogen isotherm by the BJH.

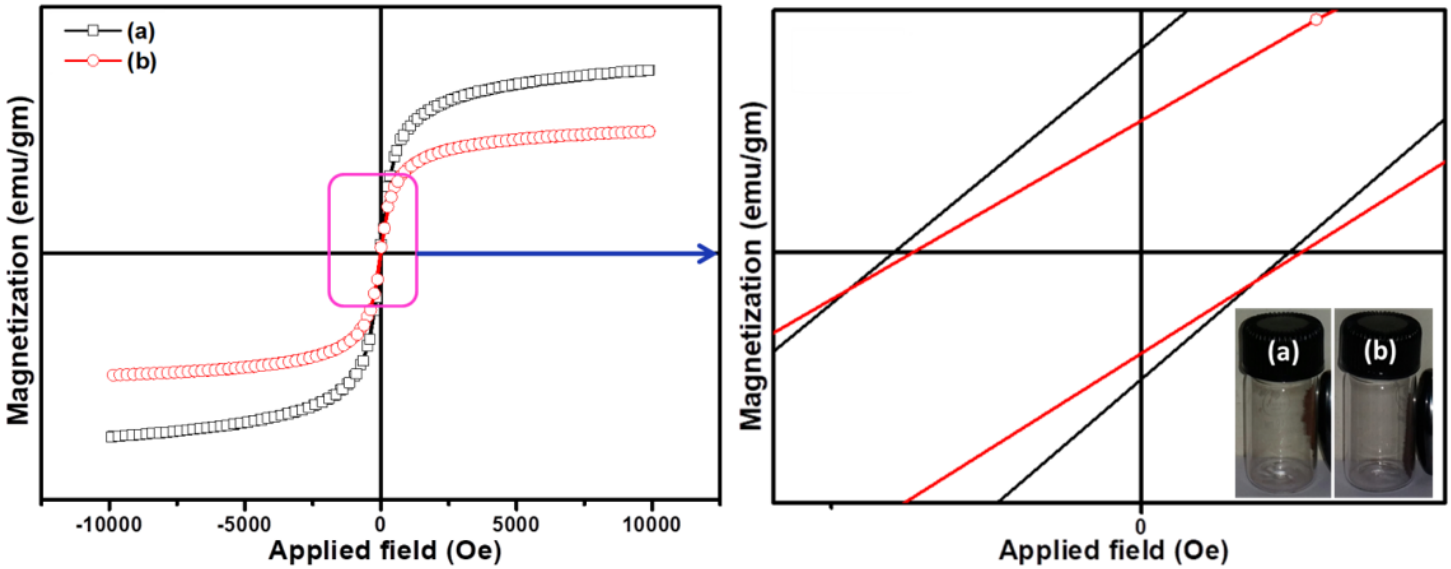

Figure 8

Magnetization curves of (a) Fe3O4 and (b) Fe3O4@SiO2@PO43-.

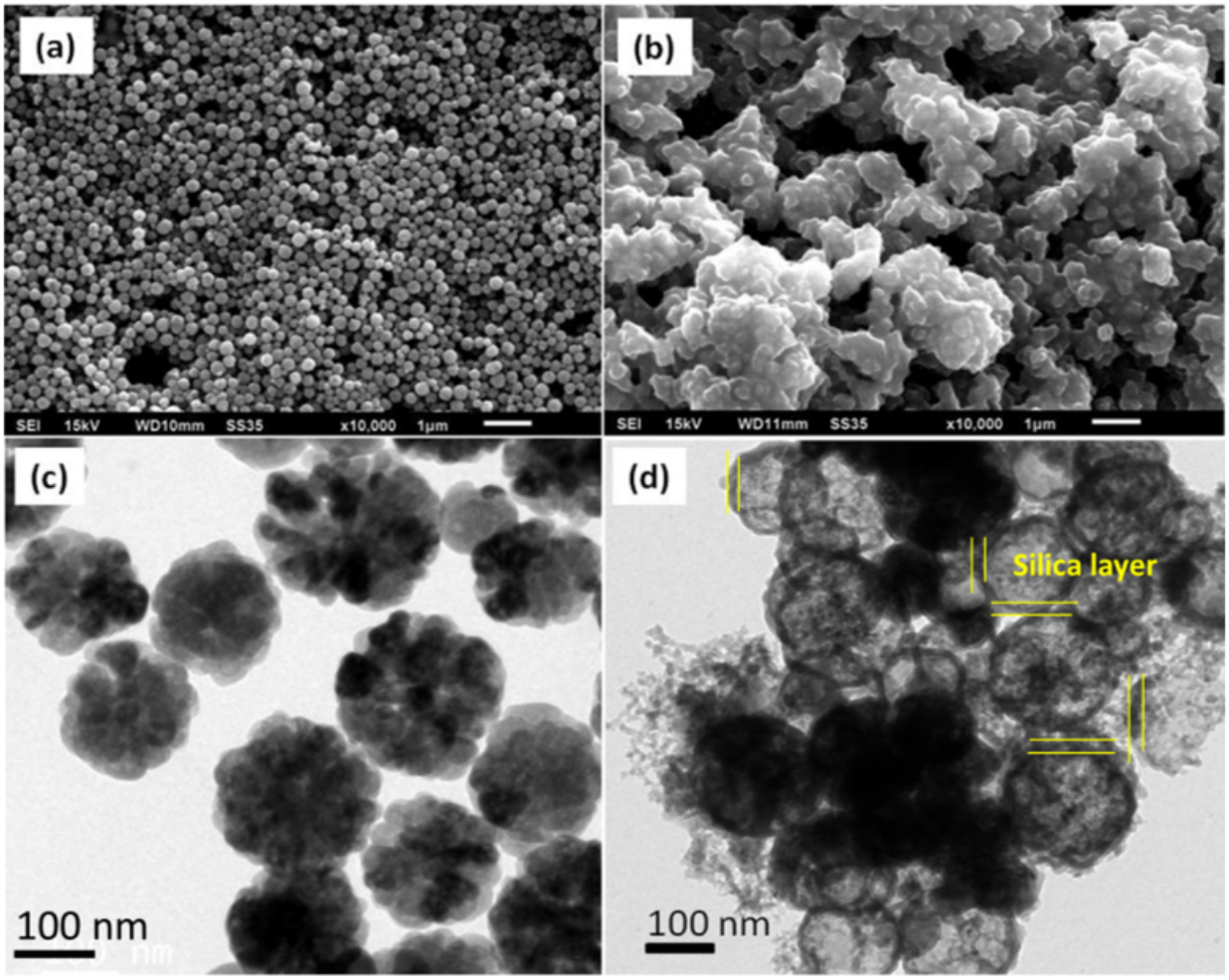

Figure 9

SEM images of (a) Fe3O4 and (b) Fe3O4@SiO2@PO43-, and TEM images of (c) Fe3O4 and (d) Fe3O4@SiO2@PO43-.

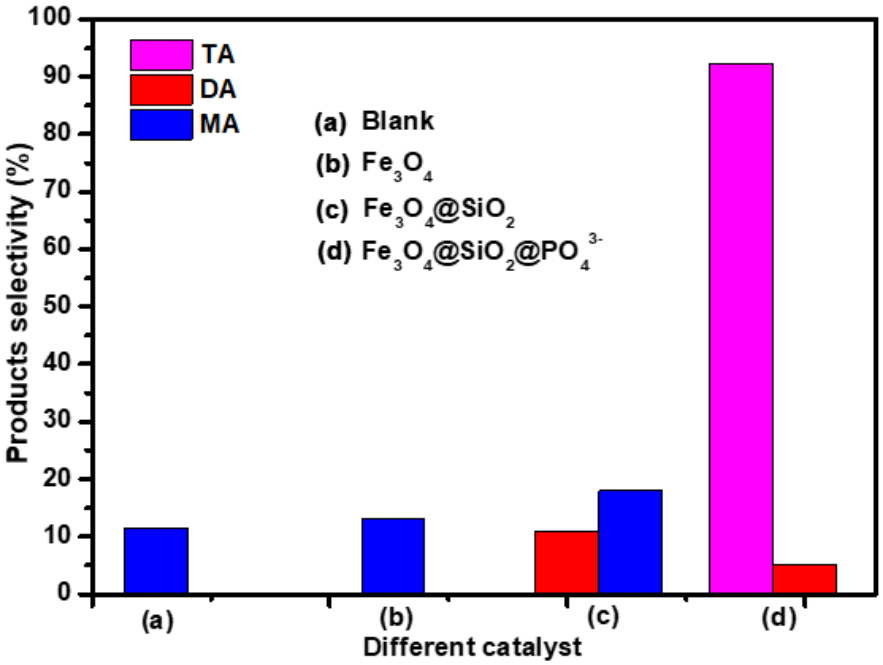

Figure 10

Effect of the various catalysts over the esterification of glycerol. [Reaction conditions: AcA/GL molar ratio = 6:1, catalyst amount = 5 wt% (with respect to GL), 80 °C = reaction temperature, and reaction time = 80 min]

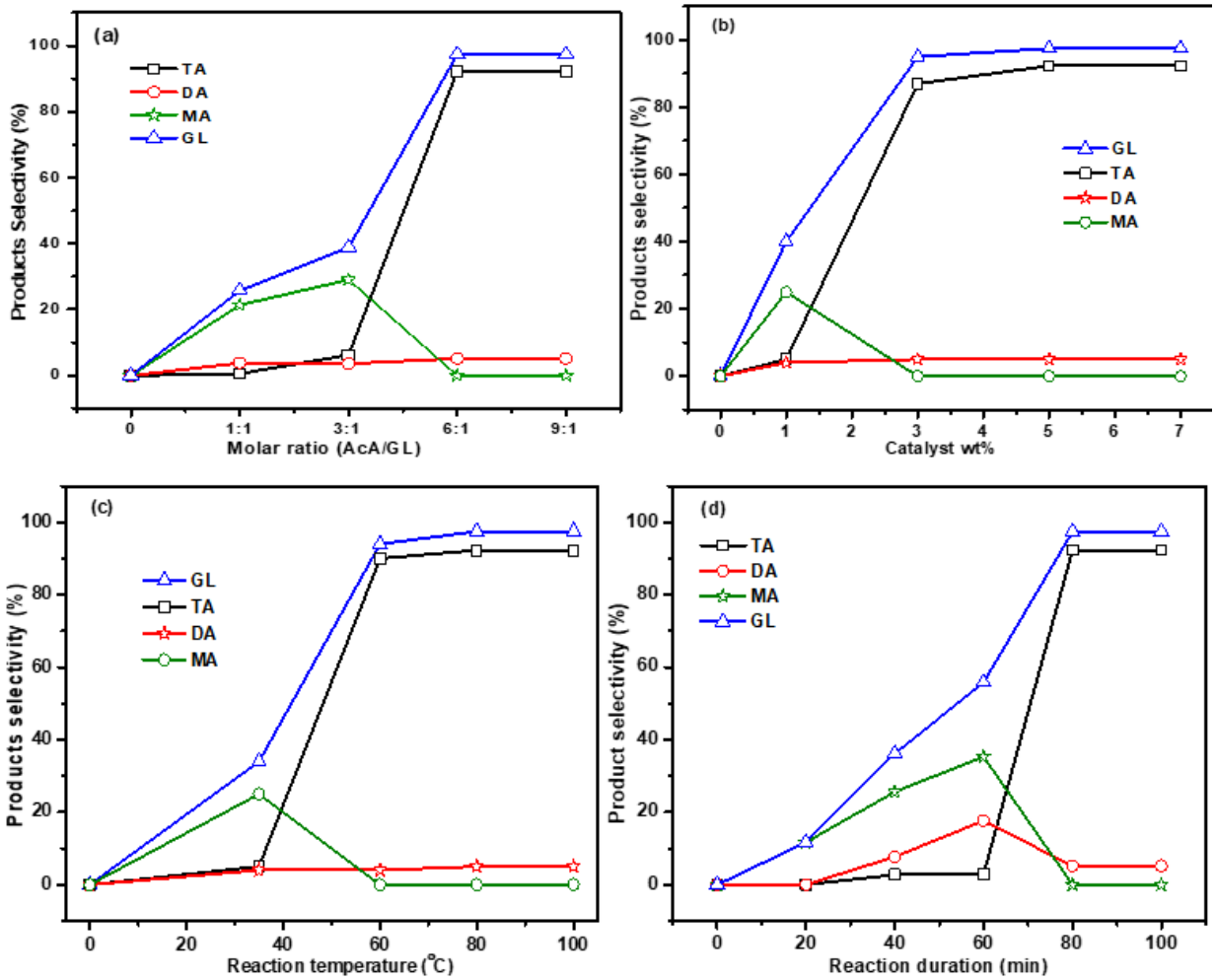

Figure 11

Effect of the various reaction parameters on GL esterification: (a) AcA/GL molar ratio, (b) catalyst amount, (c) reaction duration and (d) reaction temperature.

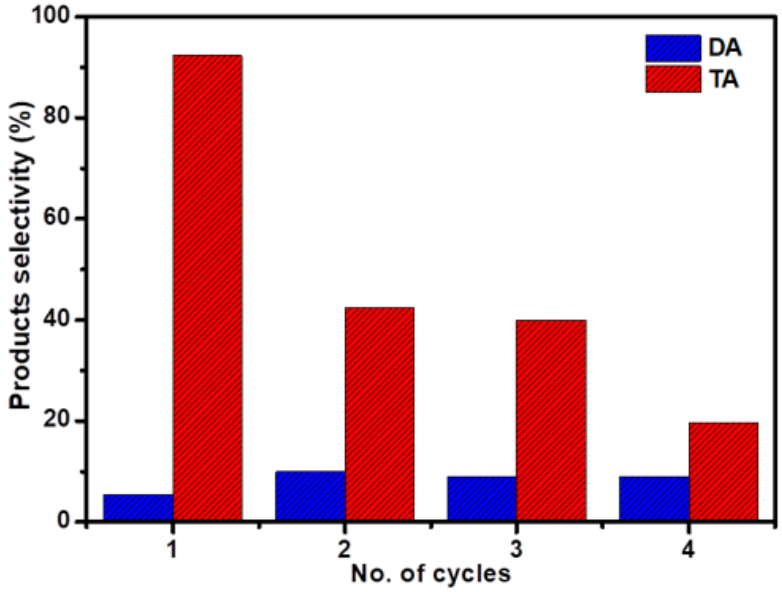

Figure 12

Study of the Fe3O4@SiO2@PO43- reusability during the glycerol esterification with acetic acid. [Reaction conditions: AcA/GL molar ratio = 6:1, catalyst amount = 5 wt% (with respect to GL), 80 °C = reaction temperature, and reaction time = 80 min]

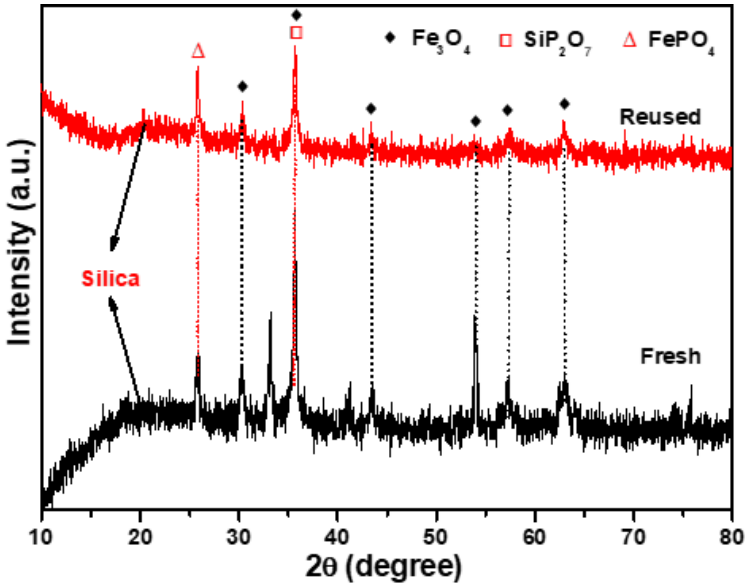

Figure 13

Comparison of XRD spectra of fresh and reused catalyst.

Supplementary Files

This is a list of supplementary files associated with this preprint. Click to download.

- SCHEME1.png
- SCHEME2.png
- SCHEME3.png
- SupplementaryInformationS.docx